

Received March 1, 2019, accepted March 26, 2019, date of publication March 29, 2019, date of current version April 16, 2019.

Digital Object Identifier 10.1109/ACCESS.2019.2908348

Axial-Flux PM Disk Generator With Magnetic Gear for Oceanic Wave Energy Harvesting

O. DOBZHANSKYI¹, EKLAS HOSSAIN¹, (Senior Member, IEEE), EBRAHIM AMIRI², R. GOUWS³, V. GREBENIKOV⁴, L. MAZURENKO⁴, M. PRYJMAK⁴, AND R. GAMALIYA⁴

¹Department of Electrical Engineering and Renewable Energy, Oregon Institute of Technology, Klamath Falls, OR 97601, USA

²Department of Electrical Engineering, University of New Orleans, New Orleans, LA 70148, USA

³Electrical and Electronic Engineering, North-West University, Potchefstroom 2531, South Africa

⁴Institute of Electrodynamics, The National Academy of Sciences of Ukraine, 01030 Kyiv, Ukraine

Corresponding author: Eklas Hossain (eklas.hossain@oit.edu)

ABSTRACT Magnetic gears (MGs) offer many advantages over mechanical ones due to their contactless mechanism of torque transfer. With the flourish of this new avenue of research, a new breed of MGs has been designed that are well suited to execute high-torque direct-drive operations. This paper investigates the performance characteristic of a disk generator located on the same shaft with an MG for oceanic wave energy harvesting application. The permanent magnets (PMs) of both the generator and the MG are arranged in a special manner to boost the overall performance of the system. To verify the validity of the proposed model, simulations of the magnetic disk gears are performed using Maxwell version 16. The calculation of the magnetic field, and the characteristics of the generator is made using Infolytica Magnet software package. Furthermore, the prototype sample of the generator with the magnetic gear is fabricated and tested in the laboratory, which further substantiates our claim.

INDEX TERMS Generator, magnetic gear, oceanic wave energy, permanent magnet, wave energy harvesting, torque density.

I. INTRODUCTION

As the conventional sources of energy are depleting, renewable energy will surely play a crucial role for the fate of humankind in the near future. In this grim context, certain avenues of research in this field are manifesting potential, oceanic wave energy being one of them. Waves are the product of wind blowing over the surface of the ocean. In certain regions of the world, the wind flow is consistent and forceful enough as to provide constant waves along the shoreline. This continuous battery of waves can be detrimental to the shoreline as it contributes to erosion. However, we can leverage these waves for the benefit of humanity. Oceanic waves contain in them tremendous energy potential which can be converted to electrical power [1]. Wave power devices are used to this end. They extract energy from the surface motion of ocean waves or from fluctuations in pressure below the surface [2].

The wave energy devices being developed and tested today are highly diverse and a variety of technologies has been

proposed to capture the energy from waves. Some of the more promising designs are undergoing demonstration testing at commercial scales. To extract electric energy from oscillating sea waves, wave energy is first converted into kinetic and then electric energy by using wave impulse electrical installations with low to medium power ($P = 150 - 3000 \text{ W}$) generators. With an average wind speed of $V = 3 - 5 \text{ m/s}$, the operating speed range of the wind power generators is approximately $n = 100 - 500 \text{ rpm}$ [3]. Direct drive low-speed power generator with the speed range of $n = 100 - 500 \text{ rpm}$ is quite large in terms of dimensions, and relatively costly. Mechanical gearboxes could effectively increase the rotating frequency of the generator and, thereby, reduce the mass of its active parts. However, mechanical gearboxes are the source of additional noise and thus require regular maintenance.

The available literature explores a number of approaches to circumvent the use of mechanical gearboxes. Magnetic gears (MG) are a promising technology as they offer several advantages over mechanical gears. MG devices do not create additional noise, do not require lubrication, and are more durable as opposed to mechanical gearboxes [4]. In [5], Li *et al.* have successfully demonstrated that field-modulated

The associate editor coordinating the review of this manuscript and approving it for publication was Haiyong Zheng.

magnetic gears can be considered as feasible and even preferable alternatives to mechanical gearboxes for certain applications due to their comparatively higher torque density. However, magnetic gears are not without their drawbacks, axial leakage flux being a prominent one. If this phenomenon is not accounted for, this can result in an overestimation of torque density. Reduced torque can also be a challenge to accurate modeling of a magnetic gear. A refined quasi-analytical 3D method to model the field distribution of axial flux magnetic gear has been proposed in [6] that overcomes the limitations of 2D analytical methods. In addition, more innovative designs and methods have been explored to better leverage the contactless torque transfer mechanism offered by magnetic gears. One such design is the novel non-rare-earth axial-field magnetic variable gear [7], which provides a way to independently magnetize the various PM pieces to form different pole-pair numbers. On the other hand, [8] studies the torque density characteristics in a magnetic gear constructed of rare-earth magnets. Magnetically geared PM machine topologies with inner rotor [9] and outer stator [10] are worth mentioning. In [11], Gerber and Wang provided proper definition of cogging torque to observe the effect of load angle in machine design. They also assessed two means of FEA for facilitating movement simulation in [12]. Concentric planetary magnetic gears have been explored, where attempts have been made for making them industrially feasible, by applying winding function theory (WFT) [13], and by using passive methods of oscillation repression [14]. Different design aspects of trans-rotary magnetic gear (TROMAG) were analyzed in [15] and [16], which were further integrated with electrical machines to inspect the viability of their application [17], [18]. Substantial studies were performed on coaxial radial magnetic gears in [19]–[22]. Radial flux and axial flux coaxial magnetic gears were differentiated in [23] where it was evident that as the permissible active outer radius is increased, the achievable volumetric torque density (VTD) of axial flux gears accelerates faster than the radial counterpart does. The encouraging designs of generators using axial flux and disc-type magnetic gear were investigated in [24] and [25] respectively. The significance of Halbach arrays has been studied in [26], which can improve the performance of the axial flux magnetic gears. Researchers have developed a 2D analytical model to better compute the magnetic field distribution in an axial-field magnetic gear [27]. Even more novelties in design, methods and analysis have been introduced in [28] and [29] that encapsulate the tinkering capabilities of researchers.

Magnetic gears have been integrated to several wind power generation devices [28], [30]–[32] and many marine energy converter devices such as heaving buoy wave energy converter [33]. Magnetic geared devices can prove advantageous for such applications for their low noise and vibration, improved reliability, accurate peak torque transmission capability and proper isolation between shafts [34]. Linear PM generators for application in Archimedes Wave Swing (AWS) were explored in [35]–[37]. An approach to design a

hermetically sealed MG was evaluated in [38], whereas the use of large-scale inner stator radial flux MGM was brought into consideration in [39]. In [40], Uppalapati *et al.* examined the performance of ferrite magnets in MG for low speed marine power generation.

This paper investigates the performance characteristic of a disk generator unified with a magnetic gear for oceanic wave energy harvesting application. One of the main challenges of wave generators and associated with the gearboxes is their large weight, which results in a high cost of the machines, and becomes a burden for transportation, installation, and maintenance. In this paper, such problem is mitigated by using high-energy permanent magnets (PM) in place of electrical excitation and coupling mechanisms. The high magnetic remanence of the magnets allows storing the magnetic energy in a volume significantly smaller than that of an equivalent electromagnet. This may reduce the generator and magnetic gearbox weight by as much as 50%. As a result, the shear stress density of the PM machines is higher than that of the other types of machines. For instance, the shear stress density of the conventional induction and switched reluctance machines ranges between 20-30 kN/m², while PM machines reach 40-60 kN/m². Also, the PM machines are known for their high efficiency and reliability. A wave generator must be characterized by a low cogging torque, which creates a burden for bearing system. In this paper, significant amount of the work is dedicated to cogging torque discussion. To boost the overall performance of the system, the design of the generator/magnetic gear underwent certain optimizations which include the shape of the PMs as well as the displacement angle between the upper and lower stator disks. To verify the validity of the proposed model, a 150W generator prototype with the magnetic gear is fabricated and tested in the laboratory. The rest of the paper is organized as follows: section II presents a description of the wave impulse electrical installation. The analysis and description of the proposed electric generator along its load voltage, transient, and torque characteristics are presented in section III. Section IV presents the analysis of the magnetic gear, its corresponding field distribution, and relation between the gear ratio and rotational speed. The experimental verification of the proposed generator with magnetic gear is presented in section V. Finally, the conclusions are drawn in section VI.

II. DESCRIPTION OF THE WAVE IMPULSE ELECTRICAL INSTALLATION

There are various wave energy converter devices described in the literature [32]–[40]. The structure of the wave impulse installations described in this paper is schematically shown in Fig. 1. The body submerged underwater has a vertical arrangement, with two separate blocks; an energy converter of sea waves in the upper part, and an electric generator and a magnetic step-up gear in the lower part.

The sea wave energy converter consists of floats # 5, ratchet mechanism # 4, spring accumulator # 3, overrunning clutch # 2, and flywheel # 6. The energy accumulated in

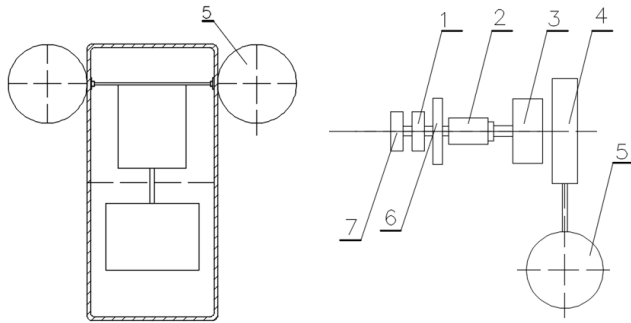


FIGURE 1. Wave impulse electrical installation. The flywheel provides smoothing of the frequency of rotation of the generator shaft. The frequency of rotation of the flywheel is within the range of 100-500 rpm.

the converter is transmitted through the shaft to the step-up reducer # 1, which is connected to the shaft of the power generator # 7. Under the action of the wave, the float moves downwards with the help of a ratchet mechanism. Also, a spring is built in the spring accumulator. After several oscillations of the wave, the spring unfastens and unwinds the flywheel, which transmits the torque to the step-up reducer, through the overrunning clutch. The flywheel provides smoothing of the frequency of rotation of the generator shaft. The frequency of rotation of the flywheel is within the range of 100-500 rpm.

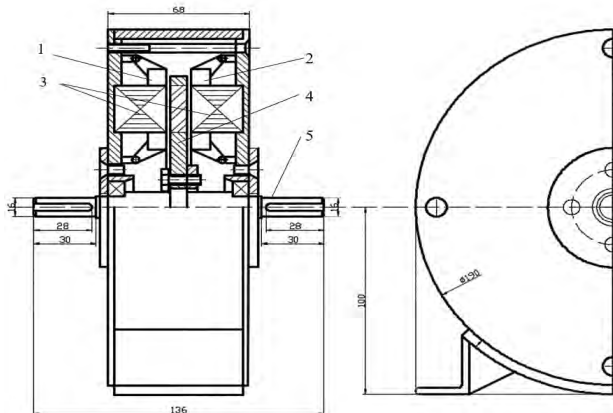


FIGURE 2. Schematic of the generator. The generator consists of a double-sided stator # 1, 2 with windings # 3 and a rotor with surface mounted (PMs) # 4. The rotor frame is fixed to the double-sided shaft # 5 and is made of a non-magnetic material, in which PMs are fixed.

III. DESCRIPTION AND ANALYSIS OF THE ELECTRIC GENERATOR

The schematic view of the generator is shown schematically in Fig. 2. The generator consists of a double-sided stator # 1, 2 with windings # 3 and a rotor with surface mounted PMs # 4. The rotor frame is fixed to the double-sided shaft # 5 and is made of a non-magnetic material, in which PMs are fixed. The technology for manufacturing the stator of such a generator is as follows: a torus is wound from isotropic electrical steel, in which the grooves for laying the coils are

milled. The stator coils are wound onto a mandrel of the corresponding profile and then placed in the grooves of the stator.

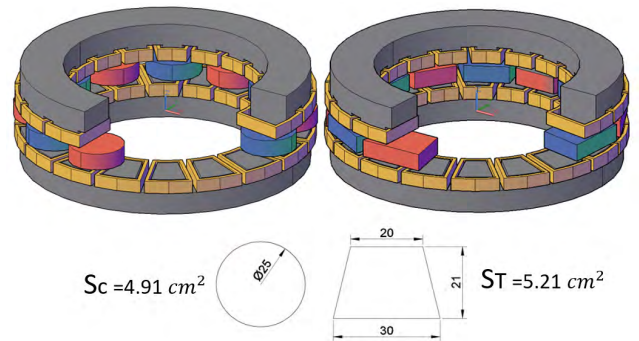


FIGURE 3. Generator with round and trapezoidal magnets. The performance of the generator may vary based on the shape (i.e. cylindrical, trapezoidal) of the PMs.

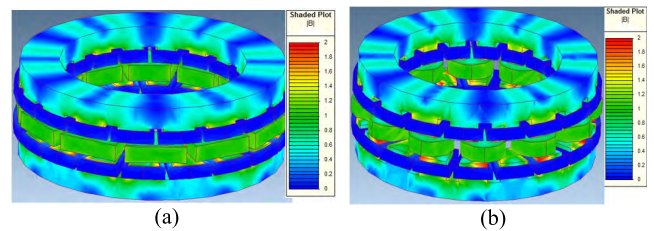


FIGURE 4. Distribution of the magnetic flux density a) trapezoidal-shaped PMs, b) cylindrical-shaped PMs.

The performance of the generator may vary based on the shape (i.e. cylindrical, trapezoidal) of the PMs (Fig. 3). Fig. 4 illustrates the distribution of the magnetic flux density inside the generator for cylindrical and trapezoidal shape PMs. The simulation results confirm that the model with trapezoidal-shaped PMs is not saturated while the model with cylindrical PMs is slightly saturated in the corners of the stator teeth.

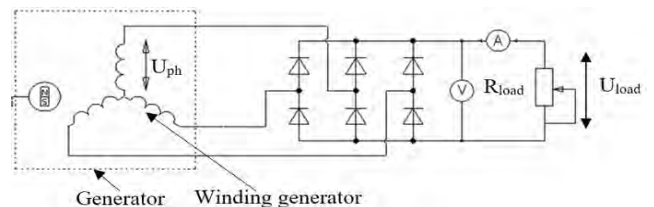


FIGURE 5. The scheme of switching the generator on the active load. The generator is connected to an active load via a rectifier bridge with six diodes.

The generator is connected to an active load via a rectifier bridge with six diodes as shown in Fig 5. The characteristic of the load voltage and the load power vs load current at the rotational speeds of $n = 1500$ rpm; $n = 2000$ rpm; and $n = 2500$ rpm, respectively, for both cylindrical and trapezoidal shaped PMs are plotted in Figs. 6 and 7.

The characteristics of a generator with trapezoidal and cylindrical magnets do not differ significantly, but the

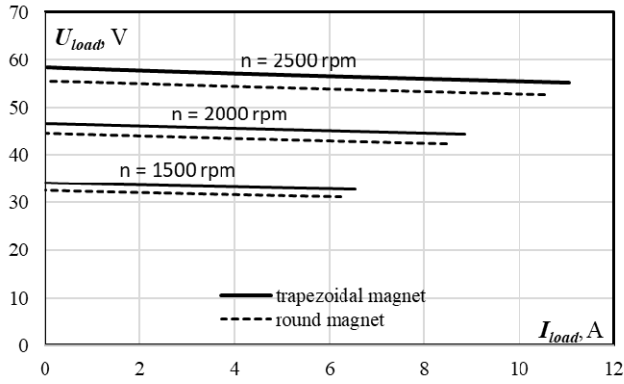


FIGURE 6. Load voltage characteristic at different speeds. It is observed that the load voltage is approximately 9% lower in the generator with cylindrical PMs, than the one with trapezoidal PMs.

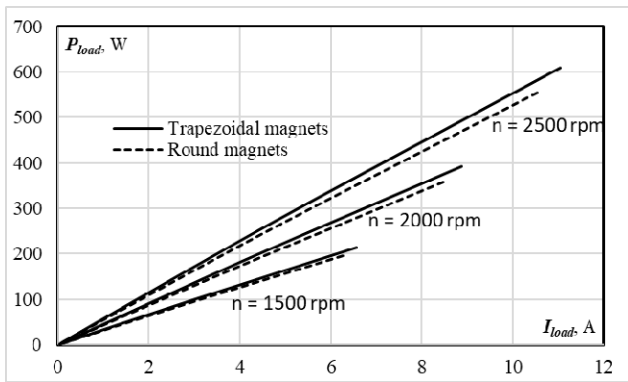
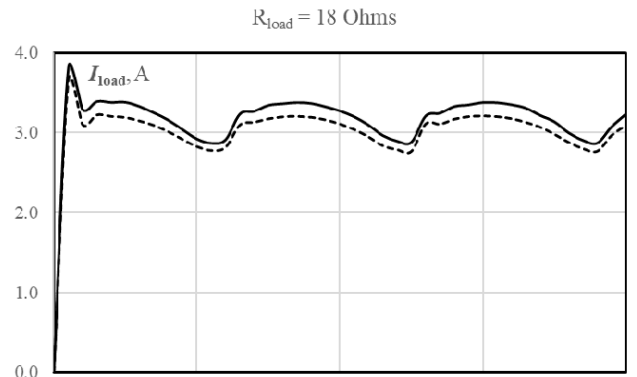


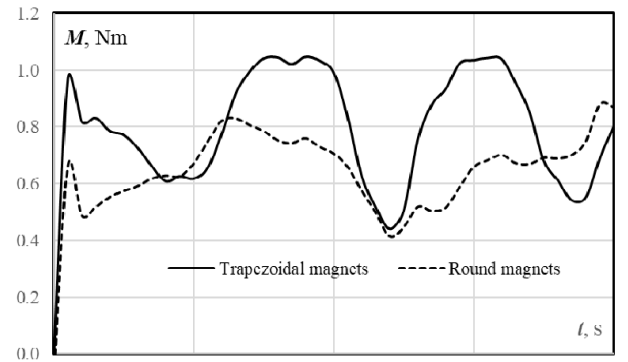
FIGURE 7. Load power characteristic for different rotational speeds. It is observed that the power is approximately 9% lower in the generator with cylindrical PMs, than the one with trapezoidal PMs.

manufacture of the rotor with magnets of the trapezoidal form has certain difficulties. This is not only due to the requirement in individual production, but also due to the execution of fastenings for magnets on the rotor, which requires a large amount of metalworking operations. It is observed that the load voltage and power are approximately 9% lower in the generator with cylindrical PMs than the one with trapezoidal PMs. This is because the area of the cylindrical PMs is smaller, and consequently, the magnetic field density in the stator with cylindrical PMs is smaller. The mass of trapezoidal PMs is larger than the mass of cylindrical PMs by 8%. Even though, the trapezoidal PMs allow the generator to produce more power than the cylindrical PMs of the same mass, it should also be noted that the cost of magnets of a cylindrical shape is lower than the cost of the trapezoidal shape magnets. In addition, the openings under the magnets are made with a standard milling cutter in one-step. Thus, manufacturing of the generator with cylindrical PMs is less expensive. Therefore, in further studies, the variant with cylindrical shape magnets was adopted as the basis.

In addition, the generator model with cylindrical PMs exhibits a better transient characteristic. Fig 8 depicts transient response of the load current and the electromagnetic torque for the two PM shapes. It can be seen that the



(a)



(b)

FIGURE 8. Transient characteristic of the generator for two different PM shapes at the rotational speed of $n = 2500$ rpm, a) load current, b) electromagnetic torque.

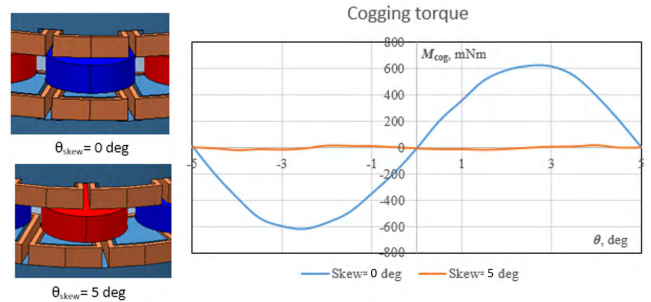


FIGURE 9. Cogging torque characteristic of the generator at zero displacement angle ($\theta_{skew} = 0^\circ$) and optimal displacement angle ($\theta_{skew} = 5^\circ$). It is observed that the cogging torque is dropped from $M_{cog-0^\circ} = 618$ mNm to $M_{cog-5^\circ} = 19$ mNm.

pulsations of the electromagnetic torque for a generator with a trapezoidal PMs are substantially higher than for the cylindrical shape. This is explained by the fact that during displacement of the rotor relative to the stator poles, the stator poles would exert less negative torque on the rotor with cylindrical-shaped PMs, leading to a smoother operation.

A 3D FEM parametric analysis of the generator was conducted for different angles between the upper and lower stator disks. Fig. 9 presents the cogging torque characteristic of the generator at zero displacement angle ($\theta_{skew} = 0^\circ$) and optimal displacement angle ($\theta_{skew} = 5^\circ$). It is observed that

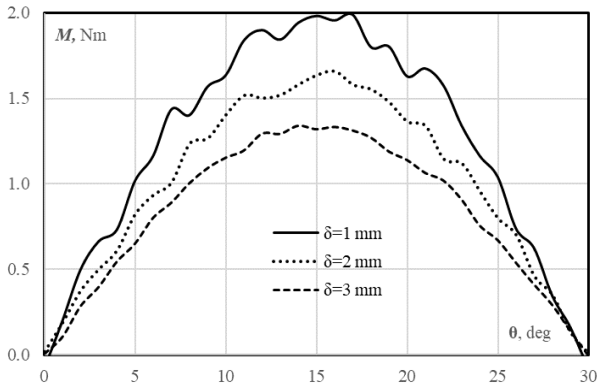


FIGURE 10. Dependency of the torque profile on the air-gap. As is seen, the electromagnetic torque pulsates more drastically at a smaller air gap. This is explained by the fact that the axial magnetic force between the PMs and the stator poles is higher at a lower air gap length.

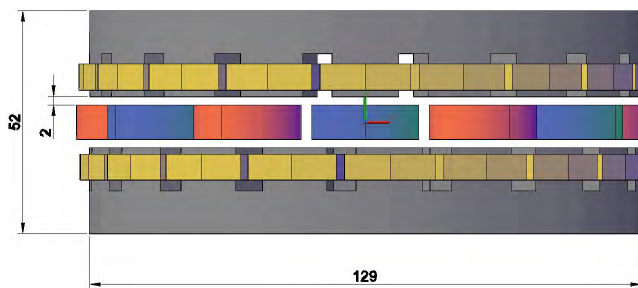


FIGURE 11. The main dimensions of the generator. All measurements are expressed in millimeter.

the cogging torque is dropped from $M_{cog-0^\circ} = 618 \text{ mNm}$ to $M_{cog-5^\circ} = 19 \text{ mNm}$. Fig. 10 displays the electromagnetic torque characteristic of the generator with three different values of the air gap. The electromagnetic torque for a 12-pole electric machine has a period of 30° (geometric degrees) and correspondingly two zero values: in the position of stable magnetic equilibrium - the axis d (this provision is taken as the initial $-\theta = 0^\circ$), and in an unstable magnetic equilibrium position - the axis q ($\theta = 30^\circ$).

As seen, the electromagnetic torque pulsates more drastically at a smaller air gap. This is explained by the fact that the axial magnetic force between the PMs and the stator poles is higher at a lower air gap length. The final design of the generator is shown in Fig. 11, with detailed design parameters listed in Table 1.

IV. DESCRIPTION AND ANALYSIS OF THE MAGNETIC GEAR

Fig. 12 present the schematic view of the disk-shaped magnetic gear with three concentric parts: high-speed rotor # 1 that is attached to the electric generator shaft, fixed steel segments # 2 and external low-speed rotor that joins the blades of the wind turbine or the wave shaft #3. PMs of high-speed and low-speed rotor are fixed on steel cores.

Fig. 13 presents the disk shaped magnetic system of the gear consisting of a high-speed and a low-speed rotor with cylindrical-shaped PMs, and fixed steel cores. The

TABLE 1. Design parameters.

Parameter	Value
Outer diameter of the generator, mm	190
Axial dimension of the generator, mm	68
Outer diameter of the stator, mm	129
Internal diameter of the stator, mm	91
Axial stator size, mm	20
Height of the stator slots, mm	10
Stator slots width, mm	7
Thickness of stator teeth, mm	15
The gap between the stator and the rotor (on each side), mm	2
Number of poles of the stator	18
Number of poles of the rotor	12
Type of permanent magnets	N38
Mass of magnets, kg	0.38
Diameter of magnets, mm	25
Thickness of magnets, mm	8
Number of stator phases	3
Number of coils per phase	6
Diameter of bare wire, mm	1.4
Cross-section of bare wire, mm ²	1.54
Number of turns of each coil	7

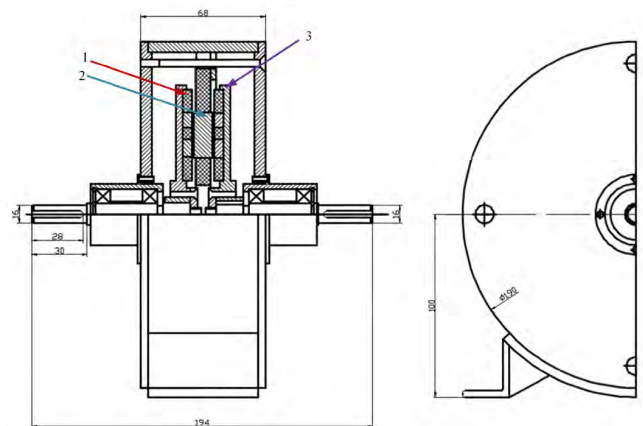


FIGURE 12. Schematic of the magnetic gear. The concentric magnetic gearbox consists of an internal high-speed rotor # 1 that is combined with the electric generator shaft, fixed steel segments # 2 and external low-speed rotor that joins the blades of the wind turbine or the wave shaft #3.

magnetization direction of the PMs is indicated by the corresponding color. As noted earlier, cylindrical-shaped PMs are relatively cheaper and normally available in stock. Therefore, instead of a single trapezoidal-shaped PM, two cylindrical-shaped PMs with different diameters are used to keep the effective mass of the PMs similar to the case of trapezoidal-shaped PMs.

The gear ratio of the magnetic gear as well as the number of fixed steel segments is determined by the ratio between the number of pole pairs on the low-speed and the high-speed rotor [30]:

$$\begin{aligned}
 G_r &= p_h/p_l; \\
 \omega_h &= -G_r\omega_l, \\
 n_s &= p_l + p_h,
 \end{aligned} \tag{1}$$

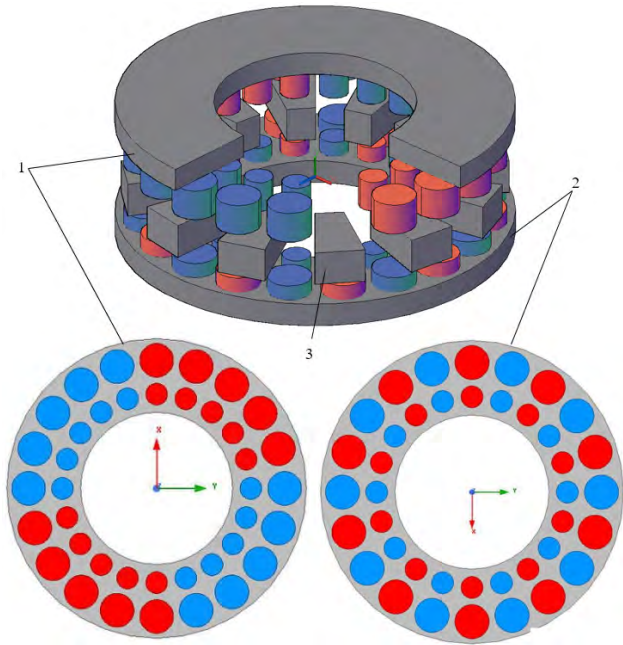


FIGURE 13. Magnetic reducer: low-speed rotor (on the right), high-speed rotor (on the left). The corresponding colors indicate the magnetization direction of the PMs.

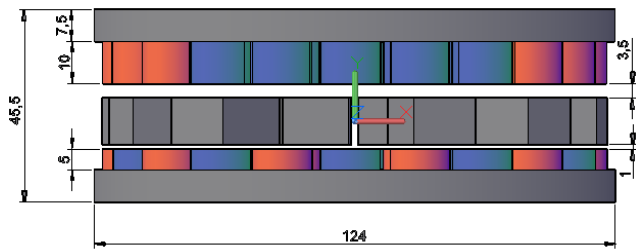


FIGURE 14. The main dimensions of the magnetic gear.

where G_r is the ratio of the magnetic reduction gear; p_l is the number of pole pairs of the low-speed rotor; p_h is the number of pole pairs of the high-speed rotor; n_s is the number of fixed steel segments; ω_l - rotational speed of the low-speed rotor; ω_h - speed of rotation of the high-speed rotor (low-speed and high-speed rotor rotate in opposite directions).

The higher the gear ratio, the higher the speed of the high speed rotor and the generator. However, for a magnetic gearbox with a large gear ratio, excessive leakage between magnets occur due to the use of a large number of poles on the high-count pole rotor. Besides, a large number of stationary steel segments with relatively small thickness are required, which may partially saturate the machine.

The main dimensions of the magnetic gear (Fig. 14) include; the height of the PMs of the high-speed $h_{(HS)}$ rotor, height of the PMs of the low-speed $h_{(LS)}$ rotor, the air-gap between the high-speed rotor and the fixed steel segments (δ_1) and the air-gap between the low-speed rotor and the fixed steel segments (δ_2). In particular, air-gap length could affect the transient start up process of the gear.

At the initial stage, numerical studies of the characteristics of the magnetic gearbox were performed for high speed $h_{(HS)}$

TABLE 2. Magnetic gear parameters.

N	$2p_{(HS)}$	$2p_{(LS)}$	δ_1 mm	δ_2 mm	$M_{(HS)max}$ Nm	$M_{(LS)max}$ Nm	$M_{(cogg)max}$ Nm
1	2	9	3.5	1	1.52	7.06	0.017
2	2	10	3.5	1	2.67	7.2	1.54
3	2	11	3.5	1	1.57	8.66	0.013
4	2	9	2	2	1.45	6.46	0.048
5	2	10	2	2	3.26	7.11	2.53
6	2	11	2	2	1.38	7.51	0.026
7	2	9	1	1	2.12	9.28	0.065
8	2	10	1	1	5.15	10.61	3.78
9	2	11	1	1	2.02	11.11	0.019

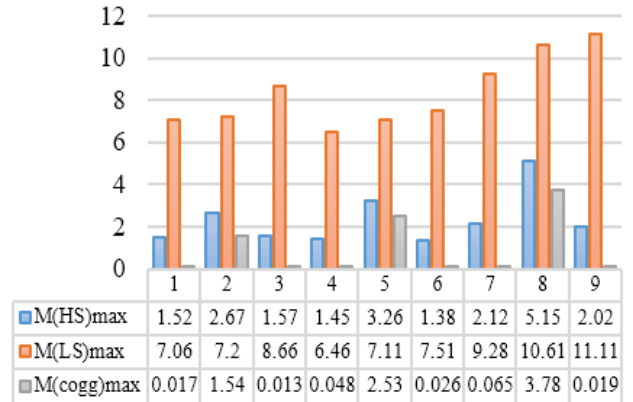


FIGURE 15. Maximal values of torque for high and low speed rotors.

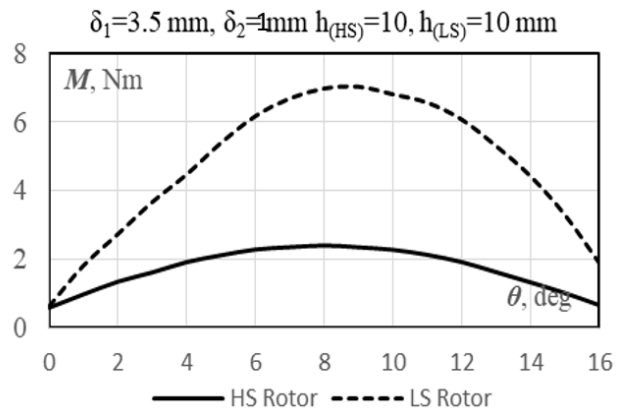


FIGURE 16. The torque acting on the high-speed and low-speed rotor. The main dimensions of the magnetic gear include; the height of the PMs of the high-speed $h_{(HS)}$ rotor, height of the PMs of the low-speed $h_{(LS)}$ rotor, the air-gap between the high-speed rotor and the fixed steel segments (δ_1) and the air-gap between the low-speed rotor and the fixed steel segments (δ_2). In particular, air-gap length could affect the transient start up process of the gear.

and low speed $h_{(LS)}$ rotors with the following dimensions: $h_{(HS)} = 10$ mm, $h_{(LS)} = 10$ mm; $h_{(HS)} = 5$ mm, $h_{(LS)} = 5$ mm; $h_{(HS)} = 10$ mm, $h_{(LS)} = 5$ mm. As a result of these studies, it was found that the following ratio of rotor height: $h_{(HS)} = 10$ mm, $h_{(LS)} = 5$ mm, which was taken as the basis for further research, is optimal in terms of the mass of magnets and the maximum electromagnetic torque on a high-speed rotor.

At the second stage of numerical studies, the number of pole-pairs on the low-speed rotor ($2p_{(LS)}$) and the air-gap

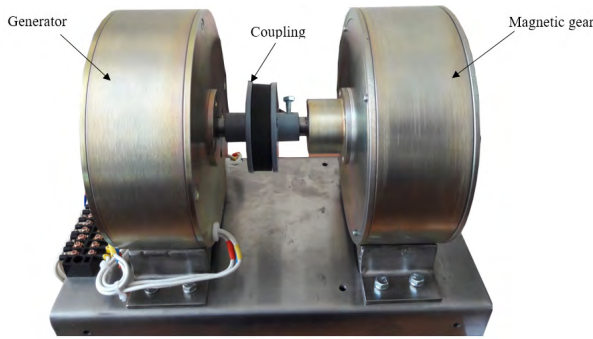


FIGURE 17. The prototype of the generator and the magnetic gear. On the left, we have the generator whose windings are connected to a special terminal block. On the right is the magnetic gearbox, which is coupled with a generator by means of a clutch.

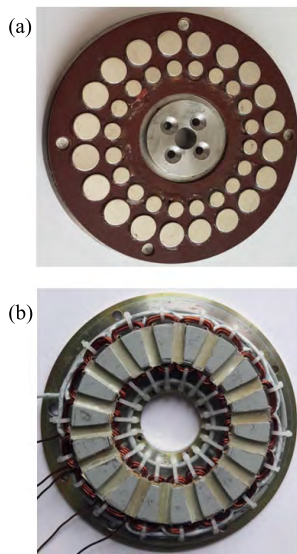


FIGURE 18. a) A physical model of the high-speed rotor of the gear. b) The physical model of the stator the generator.

(δ_1) and (δ_2) were varied. For the various ratios of pole pairs and the air-gaps, the maximum electromagnetic torque of the high speed ($M_{(HS)max}$) and the low speed ($M_{(LS)max}$) rotors, as well as the maximum torque ($M_{(cog)max}$) were determined. The torque moment of a magnetic gearbox, for example, acting on a high speed rotor in a predetermined position of the rotor α_{HS} , is defined as the torque M_{HS} required to hold the rotor in that position when the second (low speed rotor) is in the position of the steady magnetic equilibrium ($M_{LS} = 0, dM_{LS}/d\alpha_{LS}$). For each given position of the high-speed rotor, the position of the stable magnetic equilibrium for the low-speed rotor is determined and the torque value on the high-speed rotor is the desired value of the torque. In Table 2 the maximum values of torque of for high and low speed, rotors are presented. The results are graphically demonstrated in Fig. 15.

Analyzing the results, it should be noted that the cogging torque for the integer gear ratio has significantly greater value than for the non-integer ratio. The lowest value of the cogging torque for an integer gear ratio was obtained at the greater

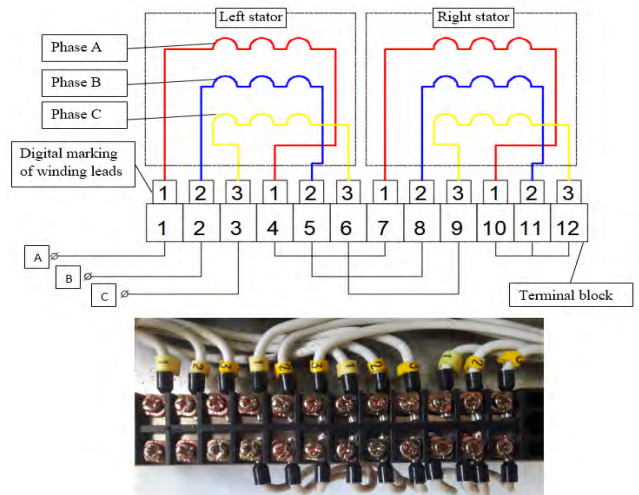


FIGURE 19. Winding ends and marking of the terminals. The coils of one phase of the “left” and “right” stators are also connected in series. The ends of all phases are connected to the terminal block and, if necessary, can be switched to the “triangle” circuit or the parallel connection of the phases of the “left” and “right” stators.

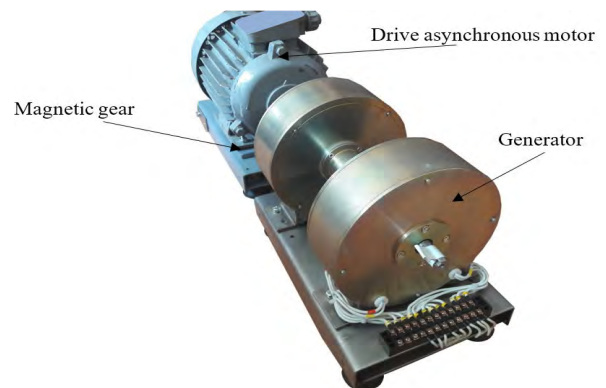


FIGURE 20. The test assembly with asynchronous motor, magnetic gear, electric generator.

air-gap value between the high-speed rotor and the stationary steel segments. With a substantially higher cogging torque value for an integer gear ratio, the value of the maximum torque for the high-speed rotor is also larger if compared to that with non-integer gear ratio. Moreover, the value of the maximum torque for all variants with non-integer values of the gear ratio do not differ significantly. The manufacture of a gearbox with an integer value of the gear ratio is much cheaper, since the non-magnetic base of both rotors is manufactured on the machine at the same time, and then the cylindrical magnets are bonded to the desired magnetization venture. Therefore, it was decided to manufacture the gearbox N2 from Table 2. For this machine the torque characteristic of the gear in both high speed and low speed rotors are plotted in Fig. 16.

V. EXPERIMENTAL VERIFICATION

The prototype of the electric generator attached to the magnetic gear is shown in Fig. 17. On the left, we have the generator whose windings are connected to a special terminal block. On the right is the magnetic gearbox, which is coupled

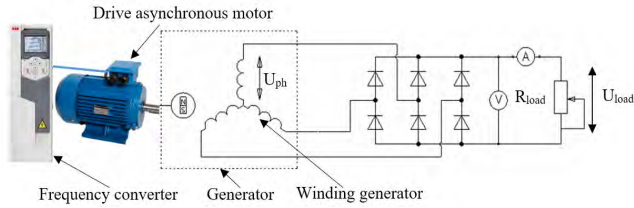
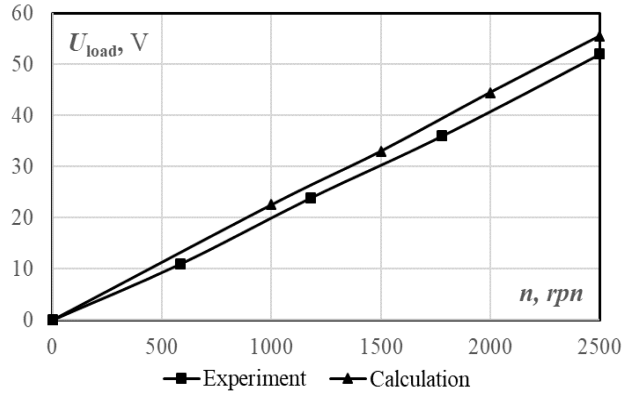
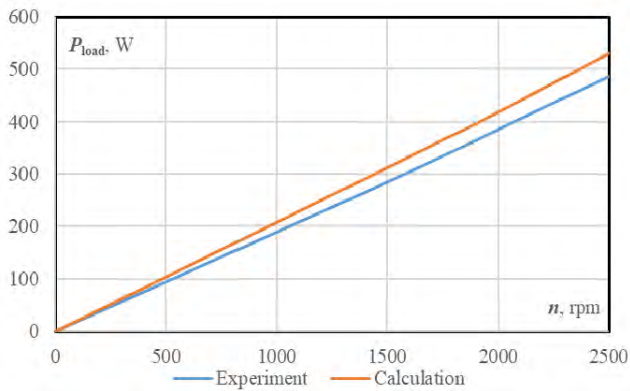


FIGURE 21. Scheme for testing the generator. As a load, a resistor (R_{load}) with variable resistance was used.



(a)

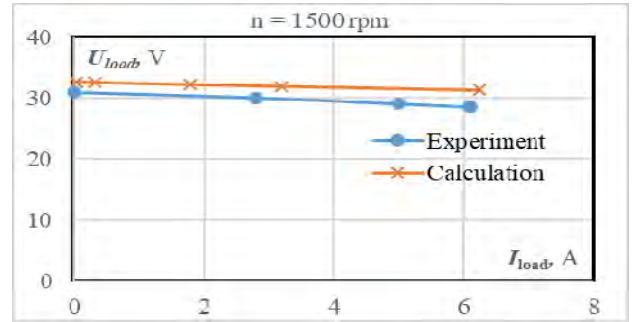


(b)

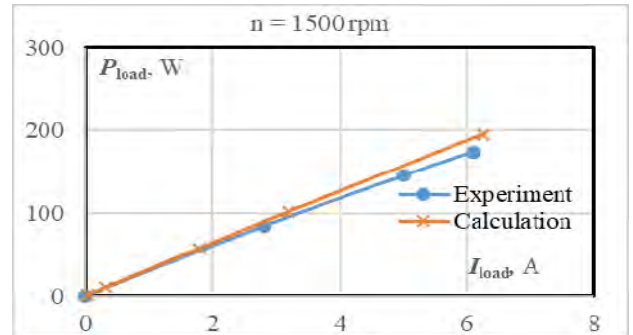
FIGURE 22. a) Load voltage characteristics, b) load power versus speed. The FEA result is slightly higher than the experimental one, mainly because factors such as losses in bearings, and fan losses during rotation of the rotor are not considered in FEA.

with a generator by means of a clutch. The general view of the high-speed rotor of the magnetic gear and the stator generator are shown in Fig. 18.

The windings were placed in the stator grooves and attached by means of bandages to special rings from the inner and outer sides. Each of the stator coils is wound with a copper wire, whose diameter without insulation is equal to $d_{wire} = 1.4$ mm, wire diameter in insulation $d_{insol} = 1.51$ mm, wire cross-section without insulation $S_{wire} = 1.54$ mm², the rated current density is $J_n = 5$ A/mm², the rated phase current is $I_n = 7.7$ A. The generator consists of 2 stators, 18 coils, and 6 coils per phase. Number of turns in each coil $W = 7$. All the coils of one phase are connected in series. The coils of one phase of the “left” and “right” stators are also connected in series. The ends of all



(a)



(b)

FIGURE 23. External characteristic of the generator a) load voltage, b) load power. The divergence observed in experimental and theoretical results can be attributed to losses in bearings and fans.

phases are connected to the terminal block and, if necessary, can be switched to the “triangle” circuit or the parallel connection of the phases of the “left” and “right” stators. The connection diagram and the marking of the terminals of the electro-generator windings are shown in Fig. 19. The number of turns and the connection scheme of the windings were selected in such a way that, at a nominal rotation frequency equal to $n = 2500$ rpm and switching on the generator windings to the load through a three-phase rectifier, the voltage was equal to $U_{load} = 50$ V in idling mode.

It should be noted that when winding the coil with a single-core wire, whose diameter is $d_{wire} = 1.4$ mm, and the size of the stator tooth is 15 mm, the slot filling factor will not be large. For better filling of the winding window, it is necessary to reel the coils with a stranded wire.

The test bench for the generator sample consists of the following main parts: frequency converter ($P_n = 22$ kW, $I_n = 45$ A) asynchronous motor ($P_n = 3.5$ kW, $n = 2780$ rpm, $I_n = 7.7$ A), generator with PM (Fig. 20). Generator windings were connected to a three-phase rectifier (Larionov’s circuit). For the Larionov scheme, the following relations are known:

$$U_{load} = 2.34 \times U_{ph}, \quad I_{load} = 1.28 \times I_{ph} \quad (2)$$

As a load, a resistor (R_{load}) with variable resistance was used. The experimental set-up for testing the generator is shown in Figs. 20 and 21. The experimental set-up was simplified if compared to the one shown in Fig. 1. Instead of using a ratchet mechanism and flywheel, the rotational force is provided to the magnetic gear by the asynchronous motor. According to

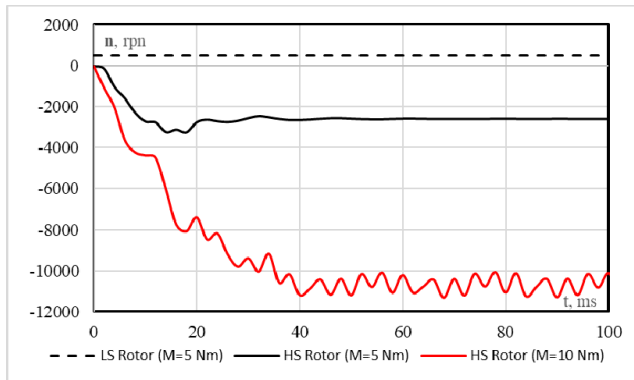


FIGURE 24. Transient speed response of the reducer under different load conditions. The transient oscillations observed in the high-speed rotor are due to the initial mutual position between the low-speed and high-speed rotor, but the two rotors get synchronized shortly after.

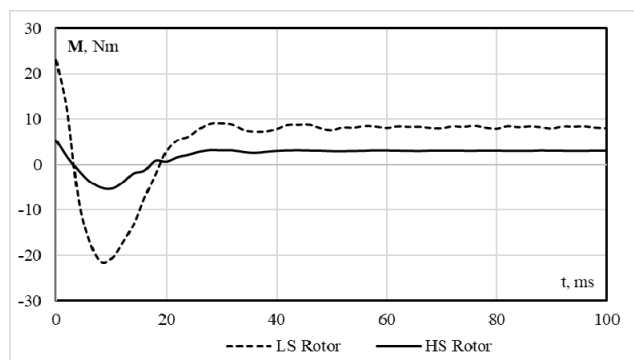


FIGURE 25. Transient torque characteristic of the gear exerted on both high speed and low-speed rotors.

Figs. 20 and 21, the characteristics of the generator coupled with the gearbox were determined as follows: with the frequency converter, the fixed speed of asynchronous motor was set and the effect of the voltage and current in the load were determined.

Fig. 22 presents the voltage and power across the load in various operating speeds. The FEA result is slightly higher than the experimental one, mainly because factors such as losses in bearings, and fan losses during rotation of the rotor are not considered in FEA.

Fig. 23 displays the characteristic of the load voltage and power to the load current. The transient speed response of the magnetic gear under different load conditions is depicted in Fig. 24. The rotational speed of the low-speed rotor is set equal to $\omega_l = 500$ rpm and the load torque is equal to $T_{load} = 5$ Nm. It can be seen that, after the transient time has passed ($t = 20$ ms), the high-speed rotor settles at the speed of $\omega_h = 2500$ rpm, which is 5 times greater than the rotational speed of the low-speed rotor. The transient oscillations observed in the high-speed rotor are due to the initial mutual position between the low-speed and high-speed rotor, but the two rotors get synchronized shortly after. When the load exceeds the torque limit ($T_{load} = 10$ Nm), the outer rotor starts to slide, and speed suddenly increases, as it can no longer be maintained at 2500 rpm (Fig. 24). The electromagnetic torque profile exerted on both high speed and low-speed rotors are plotted in Fig. 25.

VI. CONCLUSIONS

A magnetic gearbox has been unified with a disk generator for wave energy harvesting application. A prototype has been developed using cylindrical disk shaped magnetic gears. The design has been fine-tuned to improve the system performance. It was observed that the pulsations of the electromagnetic torque for an electric generator with cylindrical shaped magnets are much smaller compared to trapezoidal magnets. They are also preferable for their low cost and smaller area and magnetic field density. The model was verified by the experimental measurements of the FEA results. Proper research needs to be carried out on the scalability of this promising technology so that it can overcome the detrimental effect on the environment and provide enough power to save future generations from the exploits of oil-based economy.

REFERENCES

- [1] B. Czech and P. Bauer, "Wave energy converter concepts: Design challenges and classification," *IEEE Ind. Electron. Mag.*, vol. 6, no. 2, pp. 4–16, Jun. 2012.
- [2] A. F. O. Falcão, J. C. C. Henriques, and L. M. C. Gato, "Rotational speed control and electrical rated power of an oscillating-water-column wave energy converter," *Energy*, vol. 120, pp. 253–261, Feb. 2017.
- [3] S. Dzenzerskyi, *Alexander Tarasov*. Kiev, Ukraine: National Academy of Sciences of Ukraine, 2011.
- [4] H. Polinder, J. A. Ferreira, B. B. Jensen, A. B. Abrahamsen, K. Atallah, and R. A. McMahon, "Trends in wind turbine generator systems," *IEEE J. Emerg. Sel. Topics Power Electron.*, vol. 1, no. 3, pp. 174–185, Sep. 2013.
- [5] X. Li, K. T. Chau, M. Cheng, and W. Hua, "Comparison of magnetic-gear permanent-magnet machines," *Prog. Electromagn. Res.*, vol. 133, pp. 177–198, 2013.
- [6] S. A. Afsari, H. Heydari, and B. Dianati, "Cogging torque mitigation in axial flux magnetic gear system based on skew effects using an improved quasi 3-D analytical method," *IEEE Trans. Magn.*, vol. 51, no. 9, Sep. 2015, Art. no. 7403111.
- [7] M. Chen, K.-T. Chau, C. H. T. Lee, and C. Liu, "Design and analysis of a new axial-field magnetic variable gear using pole-changing permanent magnets," *Prog. Electromagn. Res.* vol. 153, pp. 23–32, 2015.
- [8] V. M. Acharya, J. Z. Bird, and M. Calvin, "A flux focusing axial magnetic gear," *IEEE Trans. Magn.*, vol. 49, no. 7, pp. 4092–4095, Jul. 2013.
- [9] S. Gerber and R.-J. Wang, "Design and evaluation of a magnetically geared PM machine," *IEEE Trans. Magn.*, vol. 51, no. 8, Aug. 2015, Art. no. 8107010.
- [10] P. M. Tlali, S. Gerber, and R.-J. Wang, "Optimal design of an outer-stator magnetically geared permanent magnet machine," *IEEE Trans. Magn.*, vol. 52, no. 2, Feb. 2016, Art. no. 8100610.
- [11] S. Gerber and R.-J. Wang, "Cogging torque definitions for magnetic gears and magnetically geared electrical machines," *IEEE Trans. Magn.*, vol. 54, no. 4, Apr. 2018, Art. no. 8103209.
- [12] S. Gerber and R.-J. Wang, "Evaluation of movement facilitating techniques for finite element analysis of magnetically geared electrical machines," *IEEE Trans. Magn.*, vol. 51, no. 2, Feb. 2015, Art. no. 7400206.
- [13] N. W. Frank and H. A. Toliyat, "Analysis of the concentric planetary magnetic gear with strengthened stator and interior permanent magnet inner rotor," *IEEE Trans. Ind. Appl.*, vol. 47, no. 4, pp. 1652–1660, Jul./Aug. 2011.
- [14] N. W. Frank, S. Pakdelian, and H. A. Toliyat, "Passive suppression of transient oscillations in the concentric planetary magnetic gear," *IEEE Trans. Energy Convers.*, vol. 26, no. 3, pp. 933–939, Sep. 2011.
- [15] S. Pakdelian, N. W. Frank, and H. A. Toliyat, "Principles of the trans-rotary magnetic gear," *IEEE Trans. Magn.*, vol. 49, no. 2, pp. 883–889, Feb. 2013.
- [16] S. Pakdelian, N. W. Frank, and H. A. Toliyat, "Magnetic design aspects of the trans-rotary magnetic gear," *IEEE Trans. Energy Convers.*, vol. 30, no. 1, pp. 41–50, Mar. 2015.
- [17] S. Pakdelian, Y. B. Deshpande, and H. A. Toliyat, "Design of an electric machine integrated with trans-rotary magnetic gear," *IEEE Trans. Energy Convers.*, vol. 30, no. 3, pp. 1180–1191, Sep. 2015.
- [18] S. Pakdelian, M. Moosavi, H. A. Hussain, and H. A. Toliyat, "Control of an electric machine integrated with the trans-rotary magnetic gear in a motor drive train," *IEEE Trans. Ind. Appl.*, vol. 53, no. 1, pp. 106–114, Jan./Feb. 2017.

- [19] M. Johnson, M. C. Gardner, and H. A. Toliyat, "A parameterized linear magnetic equivalent circuit for analysis and design of radial flux magnetic gears—Part I: Implementation," *IEEE Trans. Energy Convers.*, vol. 33, no. 2, pp. 784–791, Jun. 2018.
- [20] M. Gardner, M. Johnson, and H. A. Toliyat, "Analysis of high gear ratio capabilities for single-stage, series multistage, and compound differential coaxial magnetic gears," *IEEE Trans. Energy Convers.* to be published.
- [21] M. Johnson, M. C. Gardner, and H. A. Toliyat, "Design comparison of NdFeB and ferrite radial flux surface permanent magnet coaxial magnetic gears," *IEEE Trans. Ind. Appl.*, vol. 54, no. 2, pp. 1254–1263, Mar./Apr. 2018.
- [22] M. C. Gardner, B. E. Jack, M. Johnson, and H. A. Toliyat "Comparison of surface mounted permanent magnet coaxial radial flux magnetic gears independently optimized for volume, cost, and mass," *IEEE Trans. Ind. Appl.*, vol. 54, no. 3, pp. 2237–2245, May/Jun. 2018.
- [23] M. C. Gardner, M. Johnson, and H. A. Toliyat, "Comparison of surface permanent magnet axial and radial flux coaxial magnetic gears," *IEEE Trans. Energy Convers.*, vol. 33, no. 4, pp. 2250–2259, Dec. 2018.
- [24] M. Johnson, M. C. Gardner, and H. A. Toliyat, "Design and analysis of an axial flux magnetically geared generator," *IEEE Trans. Ind. Appl.*, vol. 53, no. 1, pp. 97–105, Jan./Feb. 2017.
- [25] R.-J. Wang, L. Brönn, S. Gerber, and P. M. Tlali, "Design and evaluation of a disc-type magnetically geared PM wind generator," in *Proc. 4th Int. Conf. Power Eng., Energy Elect. Drives*, May 2013, pp. 1259–1264.
- [26] M. Johnson, M. C. Gardner, and H. A. Toliyat, "Analysis of axial field magnetic gears with halbach arrays," in *Proc. IEEE Int. Electr. Mach. Drives Conf. (IEMDC)*, May 2015, pp. 108–114.
- [27] T. Lubin, S. Mezani, and A. Rezzoug, "Development of a 2-D analytical model for the electromagnetic computation of axial-field magnetic gears," *IEEE Trans. Magn.*, vol. 49, no. 11, pp. 5507–5521, Nov. 2013.
- [28] L. Jian, G. Xu, Y. Gong, J. Song, J. Liang, and M. Chang, "Electromagnetic design and analysis of a novel magnetic-gear-integrated wind power generator using time-stepping finite element method," in *Proc. Prog. Electromagn. Res.*, Feb. 2011, pp. 351–367.
- [29] R. Holehouse, K. Atallah, and J. Wang, "Design and realization of a linear magnetic gear," *IEEE Trans. Magn.*, vol. 47, no. 10, pp. 4171–4174, Oct. 2011.
- [30] L. Jian, K. T. Chau, and J. Z. Jiang, "A magnetic-geared outer-rotor permanent-magnet brushless machine for wind power generation," *IEEE Trans. on Ind. Appl.*, vol. 45, no. 3, pp. 954–962, May/Jun. 2009.
- [31] R.-J. Wang and S. Gerber, "Magnetically geared wind generator technologies: Opportunities and challenges," *Appl. Energy*, vol. 136, pp. 817–826, Dec. 2014.
- [32] O. Dobzhanskyi, E. Amiri, R. Gouws, V. Grebenikov, L. Mazurenko, and M. Pryjmak, "Permanent magnet axial flux generator with magnetic reducer for wind and wave energy conversion systems," *IEEE Trans. Magn.* to be published.
- [33] W. Li, K. T. Chau, and J. Z. Jiang, "Application of linear magnetic gears for pseudo-direct-drive oceanic wave energy harvesting," *IEEE Trans. Magn.*, vol. 47, no. 10, pp. 2624–2627, Oct. 2011.
- [34] K. Atallah, S. D. Calverley, and D. Howe, "Design, analysis and realisation of a high-performance magnetic gear," *IEEE Proc. Electr. Power Appl.*, vol. 151, no. 2, pp. 135–143, Mar. 2004.
- [35] H. Polinder, B. C. Mecrow, A. G. Jack, P. Dickinson, and M. A. Mueller, "Conventional and TFPM linear generators for direct-drive wave energy conversion," *IEEE Trans. Energy Convers.*, vol. 20, no. 2, pp. 260–267, Jun. 2005.
- [36] H. Polinder, M. E. C. Damen, and F. Gardner, "Linear PM generator system for wave energy conversion in the AWS," *IEEE Trans. Energy Convers.*, vol. 19, no. 3, pp. 583–589, Sep. 2004.
- [37] M. Leijon et al., "Multiphysics simulation of wave energy to electric energy conversion by permanent magnet generator," *IEEE Trans. Energy Convers.*, vol. 20, no. 1, pp. 219–224, Mar. 2005.
- [38] H. Baninajar, J. Z. Bird, S. Modaresahmadi, and W. Williams, "Electromagnetic and mechanical design of a hermetically sealed magnetic gear for a marine hydrokinetic generator," in *Proc. IEEE Energy Convers. Congr. Expo. (ECCE)*, Sep. 2018, pp. 4987–4993.
- [39] M. Johnson, M. C. Gardner, H. A. Toliyat, S. Englebretson, S. Ouyang, and S. Tschida, "Design, construction, and analysis of a large-scale inner stator radial flux magnetically geared generator for wave energy conversion," *IEEE Trans. Ind. Appl.*, vol. 54, no. 4, pp. 3305–3314, Jul./Aug. 2018.
- [40] K. K. Uppalapati, J. Z. Bird, D. Jia, J. Garner, and A. Zhou, "Performance of a magnetic gear using ferrite magnets for low speed ocean power generation," in *Proc. IEEE Energy Convers. Congr. Expo. (ECCE)*, Sep. 2012, pp. 3348–3355.



O. DOBZHANSKYI is currently with the Electrical Engineering and Renewable Energy Department, Oregon Institute of Technology, Klamath Falls, OR, USA.

EKLAS HOSSAIN (M'09–SM'17) received the B.S. degree in electrical and electronic engineering from the Khulna University of Engineering and Technology, Bangladesh, in 2006, the M.S. degree in mechatronics and robotics engineering from the International Islamic University of Malaysia, Malaysia, in 2010, and the Ph.D. degree from the College of Engineering and Applied Science, University of Wisconsin Milwaukee (UWM). He has been working in the area of distributed power

systems and renewable energy integration for last ten years and he has published a number of research papers and posters in this field. He has been an Assistant Professor with the Department of Electrical Engineering and Renewable Energy, Oregon Institute of Technology, since 2015, involved with several research projects on renewable energy and grid tied microgrid system. His research interests include modeling, analysis, design, and control of power electronic devices; energy storage systems; renewable energy sources; integration of distributed generation systems; microgrid and smart grid applications; robotics, and advanced control systems. He, with his dedicated research team, is looking forward to explore methods to make the electric power systems more sustainable, cost-effective and secure through extensive research and analysis on energy storage, microgrid systems, and renewable energy sources. He is currently serving as an Associate Editor of IEEE Access. He is also a registered Professional Engineer (PE) in the state of Oregon, USA.



EBRAHIM AMIRI received the B.S. and M.S. degrees in electrical engineering from the Amirkabir University of Technology, Tehran, Iran, in 2005 and 2008, respectively, and the Ph.D. degree in electrical engineering from Louisiana State University, Baton Rouge, Louisiana, in 2013. He is currently an Assistant Professor with the Electrical Engineering Department, University of New Orleans. His current research interest includes design and optimization of electrical machinery.

R. GOUWS is currently with the Department of Electric, Electronic and Computer Engineering, North-West University, South Africa.

V. GREBENIKOV is currently with the Institute of Electrodynamics, The National Academy of Sciences of Ukraine, Kiev, Ukraine.

L. MAZURENKO is currently with the Institute of Electrodynamics, The National Academy of Sciences of Ukraine, Kiev, Ukraine.

M. PRYJMAK is currently with the Institute of Electrodynamics, The National Academy of Sciences of Ukraine, Kiev, Ukraine.

R. GAMALIYA is currently with the Institute of Electrodynamics, The National Academy of Sciences of Ukraine, Kiev, Ukraine.

• • •